Biogeosciences Discuss., https://doi.org/10.5194/bg-2017-361
Manuscript under review for journal Biogeosciences
Discussion started: 26 September 2017

Mechanisms of the Sea-Air CO_2 Flux Seasonal Cycle biases in CMIP5 Earth Systems Models in the Southern Ocean

Mongwe N. Precious[1,2]., Vichi Marcello[2,3] & Monteiro Pedro M.S.[1,2]

[1]Southern Ocean Carbon-Climate Observatory (SOCCO), CSIR, Cape Town, South Africa

[2]Oceanography of Department, University of Cape Town, Cape Town, South Africa

[3]Marine Research Institute, University of Cape Town, Cape Town, South Africa

pmongwe@csir.co.za

Abstract

The Southern Ocean forms a key component of the global carbon cycle. Recent studies, however, show that CMIP5 Earth System Models (ESM) disagree on the representation of the seasonal cycle of the CO_2 flux (FCO_2) and compare poorly to observations in the Southern Ocean. This model-observations bias has important implications on the ability of ESMs to predict century scale CO_2 sink and related climate feedbacks. In this study, we used a specialized diagnostic analysis on 10 CMIP5 models in the Southern Ocean to discriminate the role of the major drivers, namely the temperature control and the concentration of dissolved inorganic carbon (DIC). Our analysis shows that the FCO_2 biases in CMIP5 models cluster in two major groups . Group A models (MPI-ESM-MR, NorESM2 and HadGEM-ES) are characterized by exaggerated primary production such that biologically driven DIC changes mainly regulate the seasonal cycle of FCO_2. Group-B (CMCC-CESM, GFDL-ESM2M, IPSL-CM5A-MR, MRI-ESM, CanESM2, CNRS-CERFACS) overestimates the role of temperature and thus the change in CO_2 solubility becomes a dominant driver of FCO_2 variability. While CMIP5 models mostly show a singular dominant influence of these two extremes, observations show a modest influence of both, with a dominance of DIC regulation. We found that CMIP5 models overestimate cooling and warming rates during autumn and spring with respect to observations. Because of this, the role of solubility is overestimated, particularly during these seasons (autumn and spring) in group B models, to the extent of contradicting the biological CO_2 uptake during spring. Group A does not show this solubility driven bias due to the overestimation of DIC draw down. This finding strongly implies that the inability of the CMIP5 ESMs to resolve CO_2 biological uptake during spring might be crucially related to the sensitivity of the pCO_2 to temperature in addition to underestimated biological CO_2 uptake.

1. Introduction

The Southern Ocean takes up about a third of the total oceanic CO_2 uptake, slowing down the accumulation of CO_2 in the atmosphere (Fung et al., 2005; Le Quere et al., 2016; Takahashi et al., 2012). The combination of upwelling deep ocean circumpolar waters, rich in carbon and nutrients, and the subduction of fresh and colder mid-latitude waters makes it a key region in the role of sea-air exchange (Barbero et al., 2011; Gruber et al., 2009; Sallée et al., 2013). The Southern Ocean supplies about a third of the total nutrients responsible for biological production north of 30^{o}S (Sarmiento et al., 2004), and accounts for about 75% of total oceanic heat uptake (Frölicher et al., 2015). The century scale evolution of the Southern Ocean CO_2 sink is expected to change as a result of anthropogenic warming (Leung et al., 2015; Roy et al., 2011; Sarmiento et al., 1998; Segschneider and Bendtsen, 2013), however the anticipated change is still disputed. While some studies suggest that the Southern Ocean CO_2 sink is weakening and will continue to do so (e.g. Le Quéré et al., 2007; Son and Gerber, 2010; Thompson et al., 2011), other recent studies infer an increasing CO_2 sink in the Southern Ocean CO_2 (Landschutzer et al., 2015; Takahashi et al., 2012; Zickfeld et al., 2008),

Although the Southern Ocean plays a crucial role as a CO_2 reservoir and regulator of nutrients and heat, it remains under-sampled, especially during the winter season (Bakker et al., 2014; Monteiro et al., 2010). Thus, we largely rely on Earth System Models (ESM), inversions and ocean models for both process understanding and future simulation of CO_2 processes in the Southern Ocean. The Coupled Model Intercomparison Project (CMIP) provides an example of such a globally organized platform (Taylor et al., 2012). Recent studies based on CMIP5 ESMs, forward and inversions models show that although CMIP5 models agree on the CO_2 annual mean sink in the Southern Ocean, they disagree on the seasonal cycle of CO_2 flux and they are out of phase with observations (e.g. Anav et al., 2013; Lenton et al., 2013).

The seasonal cycle is a major mode of variability for chlorophyll (Thomalla et al., 2011) and CO_2 in the Southern Ocean (Lenton et al., 2013). The large-scale seasonal states of sea-air CO_2 fluxes (FCO_2) in the Southern Ocean comprise the extremes of strong summer in gassing with a weaker in-gassing or even outgassing state in winter (Ref). These extremes are linked by the autumn and spring transitions. In autumn in gassing weakens linked to the increasing entrainment of sub-surface waters, which are rich in dissolved inorganic carbon (DIC) (Lenton et al., 2013; Metzl et al., 2006; Sarmiento and Gruber, 2006). During spring, from September, the onset of primary production consumes DIC at the surface and increases the ocean capacity to take up atmospheric CO_2 (Gruber et al., 2009; Le Quéré and Saltzman, 2013; Pasquer et al., 2015; Gregor et al., 2017). The increase of sea surface temperature (SST) with summer weakens the surface CO_2 solubility, which counteracts the biological uptake and reduces the CO_2 flux from the atmosphere (Lenton et al., 2013; Pasquer et al., 2015).

FCO_2 is also spatially variable in the Southern Ocean at the seasonal scale. North of 60°S is generally the main CO_2 uptake zone (Hauck et al., 2015; Sabine et al., 2004). This region forms a major part of the sub-Antarctic zone and is characterized by the confluence of upwelled, colder and nutrient-rich deep circumpolar water and mid-latitudes warm water (McNeil et al., 2007; Sallée et al., 2006) . This region shows an enhancement of biological uptake in addition to increased CO_2 solubility due to cooler surface waters (Marinov et al., 2006; Metzl, 2009; Takahashi et al., 2012). South of 60°S towards the marginal ice zone, the flux is largely dominated by CO_2 outgassing, driven by the upwelling of circumpolar waters rich in DIC (Matear and Lenton, 2008; McNeil et al., 2007).

The inability of CMIP5 ESM to simulate a comparable FCO_2 seasonal cycle with observations in the Southern Ocean has been the subject of recent literature (Anav et al., 2013; Kessler and Tjiputra, 2016) and the mechanisms associated with these biases are still not well understood. This model-observations disagreement highlights that the current ESMs do not adequately capture the dominant seasonal processes driving the FCO_2 in the region. It also questions the sensitivity of models to adequately predict the Southern Ocean century scale CO_2 sink and its sensitivity to climate change feedbacks (Lenton et al., 2013). Efforts to improve simulations of CO_2 properties with respect to observations in the Southern Ocean are ongoing using forced ocean models (e.g. Pasquer et al., 2015; Rodgers et al., 2014; Visinelli et al., 2016), however it remains a challenge for fully coupled simulations. In a previous study, we developed a diagnostic framework to evaluate the seasonal characteristics of the drivers of FCO_2 in ocean biogeochemical models (Mongwe et al., 2016). In this work we applied this method to investigate the processes that drive FCO_2 at the seasonal scale in 10 CMIP5 ESM, exploring the mechanisms of the observed model biases in the Southern Ocean.

2. Methods

2.1 Observations

We used the Landschützer et al (2014) FCO_2 and partial pressure of CO_2 (pCO_2) dataset as the main suite of observations to compare against models throughout the analysis. Landschützer et al (2014) data are synthesized from Surface Ocean CO_2 Atlas version 2 (SOCAT2) observations and high resolution winds using neural network techniques (Landschützer et al., 2013). Here we use this dataset as provided by

Biogeosciences Discuss., https://doi.org/10.5194/bg-2017-361
Manuscript under review for journal Biogeosciences
Discussion started: 26 September 2017

Landschützer et al (2014) on a 1° x 1° regular grid. We also used the Takahashi et al. (2009) in situ FCO_2 dataset as a complemetary source for comparison of spatial sea-air CO_2 fluxes properties in the Southen Ocean. Takahashi et al., (2009) data are comprised of a compilation of about 3 million surface measurements globally, obtained from 1970 – 2000 and corrected for reference year 2000. This dataset is used, as provided, on a 4° (latitude) x 5° (longitude) resolution.

Using monthly mean sea surface temperature (SST) and salinity from the World Ocean Atlas 2013 dataset (Locarnini et al., 2013), we reconstructed total alkalinity (Talk) using the Lee et al. (2006) formulation. We also use this dataset as the main observations platform in section 2.3. To calculate the uncertainty of the computed Talk, we compared $Talk_{calc}$ from observed ship measurements of SST and salinity in the Southern Ocean with the observed $Talk_{obs}$ from the same measurements. We found that $Talk_{calc}$ compares well with $Talk_{obs}$ (R^2 = 0.79) (Supplementary Fig. S1). We therefore used this computed monthly Talk and pCO_2 from Landschützer et al (2014) to compute DIC using the CO2SYS (Pierrot and Wallace 2006, http://cdiac.ornl.gov/ftp/co2sys/CO2SYS_calc_XLS_v2.1). For interior ocean DIC, we used the Global Ocean Data Analysis Project (GLODAP) version 1 annual means dataset (Key et al., 2004).

The monthly climatology of MLD data was taken from de Boyer Montégut et al. (2004), on a 1° x 1° grid.

2.2 CMIP5 Model data

In this study we used the 10 CMIP5 ESMs shown in Table 1. The selection criterion for these models was based on the availability of variables in the CMIP5 data portal (http://pcmdi9.llnl.gov) at the time of writing: i.e. monthly FCO_2, pCO_2, chlorophyll, surface DIC, MLD, SST, vertical temperature fields and annual DIC for the historical scenario. The analysis covers the period 1995 – 2005. Model outputs were regridded into a common 1°x1° regular grid before all calculations, except for annual mean fluxes, which were computed on the original grid for each model.

Table 1: A description of the 10 CMIP5 ESMs that were used in this analysis, showing their ocean resolution, vertical levels and the corresponding marine biogeochemical component in the ESM.

Full name and Source	Model Name	Ocean Resolution	Z-Levels	Ocean Biology	Reference
Canadian Centre for Climate Modelling and Analysis, Cananda	CanESM2	0.9°x1.4°	40 levels	NPZD	Zahariev et al., 2008

Biogeosciences Discuss., https://doi.org/10.5194/bg-2017-361
Manuscript under review for journal Biogeosciences
Discussion started: 26 September 2017

Centro Euro-Mediterraneo Sui Cambiamenti Climatici, Italy	CMCC-CESM	0.5-2°x2°	21 levels	PELAGOS	Vichi et al., 2007
Centre National de Recherches Météorologiques-Centre Européen de Recherche et de Formation Avancée en Calcul Scientifique, France	CNRM-CM5	1°	42 levels	PISCES	Séférian et al., 2013
Institut Pierre-Simon Laplace, France	IPSL-CM5A-MR	0.5-2° x 2°	31 levels	PISCES	Séférian et al., 2013
Max Plank Institute for Meteorology, Germany	MPI-ESM-MR	0.4°	40 levels	HAMOCC5.2	Ilyina et al., 2013
Community Earth System Model, USA	CESM1-BGC	0.3° x1°	60 levels	BEC	Moore et al., 2004
Norwegian Earth System Model, Norway	NorESM1-ME	0.5° x 0.9°	53 levels	HAMOCC	Tjiputra et al., 2013
Geophysical Fluid Dynamics Laboratory Earth System Model, USA	GFDL-ESM2M	0.3° x 1°	50 levels	TOPAZ2	Dunne et al., 2013
Meteorological Research Institute-Earth System Model Version 1, Japan	MRI-ESM	0.5° x 1°	51 levels	NPZD	Adachi et al., 2013
Hadley Global Environment Model 2 – Earth System, UK	HadGEM-ES	0.3° x 1°	40 levels	Diat-HadOCC	Palmer and Totterdell, 2001

2.3 Sea-Air CO_2 Flux Drivers

The ocean-atmosphere CO_2 gradient (ΔpCO_2) is known to be the main driver of FCO_2 variability (Sarmiento and Gruber, 2006; Wanninkhof et al., 2009). For this analysis we consider that atmospheric CO_2 is relatively uniform in the Southern Ocean (Fujita et al., 2003), therefore changes in surface ocean pCO_2 mostly drive FCO_2. Surface ocean pCO_2 is controlled by two key factors; temperature through solubility and DIC

Biogeosciences Discuss., https://doi.org/10.5194/bg-2017-361
Manuscript under review for journal Biogeosciences
Discussion started: 26 September 2017

concentration through mixing and biological processes (Hauck et al., 2015; Le Quéré and Saltzman, 2013). We use this conjecture as a basis to explore the drivers of the FCO_2 seasonal cycle as applied in Mongwe et al., (2016).

The temperature driven pCO_2 and DIC variability at the surface were estimated following the work of Takahashi et al. (2002) and Mongwe et al., (2016):

$$\left(\frac{\partial pCO_2}{\partial t}\right)_{SST} = \frac{\partial pCO_2}{\partial SST}\frac{\partial SST}{\partial t} = 0.0423\, pCO_2 \frac{\Delta SST}{\Delta t} \quad (1)$$

$$\left(\frac{\partial DIC}{\partial t}\right)_{SST} = \frac{DIC}{\gamma_{DIC}\, pCO_2}\left(\frac{\partial pCO_2}{\partial t}\right)_{SST} \quad (2)$$

Note that

$$\frac{1}{pCO_2}\frac{\partial pCO_2}{\partial SST} \approx 0.0423℃^{-1}$$

was used from Takahashi et al (2002). SST, DIC and pCO_2 are monthly mean values from model output and observation-based datasets and γ_{DIC} is the Revelle factor (we use a nominal value of 14 for the Southern Ocean).

To diagnose the role of temperature in FCO_2 variability, we compared the estimated rate of change of DIC with temperature in (2) with the numerically estimated total monthly rate $|\frac{\Delta DIC}{\Delta t}|$. We thus define the index

$$M_{T-DIC} = \left|\left(\frac{\partial DIC}{\partial t}\right)_{SST}\right| - \left|\frac{\Delta DIC}{\Delta t}\right| \quad (3)$$

Which is positive when the absolute value of (2) is larger than $|\frac{\Delta DIC}{\Delta t}|$, indicating that temperature is the dominant driver of the observed surface pCO_2 (and hence FCO_2) variability and it is negative when DIC variations are more likely to be responsible for the observed pCO_2 variability.

2.4 DIC Entrainment Fluxes

CO_2 uptake has been shown to weaken during the winter season in the Southern Ocean linked to the entrainment of sub-surface DIC due to MLD changes (e.g. Lenton et al., 2013; Metzl et al., 2006; Takahashi et al., 2009). DIC entrainment fluxes (F_{DIC}) at the base of the mixed layer were estimated as follow:

$$F_{T+1}^{DIC} = DIC_{sub}\frac{\Delta MLD}{\Delta T}\frac{1}{MLD_{T+1}} \quad (4)$$

$$\Delta MLD_{T+1} = MLD_{T+1} - MLD_T \quad (5)$$

$$DIC_{sub} = DIC(depth(MLD_{T+1})) \quad (6)$$

Biogeosciences Discuss., https://doi.org/10.5194/bg-2017-361
Manuscript under review for journal Biogeosciences
Discussion started: 26 September 2017

Where T is time in months and DIC_{sub} is the subsurface DIC concentration at the base of the MLD. Annual mean DIC were used here mainly because vertical DIC fields are only available in annual means at the CMIP5 portal and observations (GLODAP). However because we are mainly interested in the period autumn – winter, where the MLD ≥ 60 m in the Sub-Antarctic zone and ≥ 40 m in the Antarctic zone (Fig 6a-f), DIC seasonality is anticipated to be minimal at this depth. To evaluate the uncertainty of using annual means, we assessed DIC entrainment fluxes using a model simulation at 0.5 degrees resolution (Dufour et al., 2013) with annual and monthly mean outputs. It was found that the estimates are indeed comparable with minimal differences (not shown). It is noted as a caveat that the F_{DIC} is only a coarse estimate of these fluxes, and is intended only for the autumn-winter period when MLDs are deep.

3. Results

The Southern Ocean is here defined as south of the Sub-tropical front (STF, as defined in Orsi et al., [1995]). It is divided into two main domains, the Sub-Antarctic Zone between the STF and the Polar Front (PF) and the Antarctic Zone south of the PF. Within the Sub-Antarctic Zone and Antarctic Zone, we further partition the domain into the three main basins of the Southern Ocean i.e. Pacific, Atlantic and the Indian Ocean.

3.1 Annual climatological sea-air CO_2 fluxes

The annual mean climatological distribution of FCO_2 in the Southern Ocean is spatially variable but mainly characterized by two key features: (i) CO_2 in-gassing north of 55^{0}S (Polar Frontal zone, PFZ) within and north of the Sub-Antarctic Zone, and (ii), CO_2 out-gassing between the PFZ and the Marginal Ice Zone (MIZ) (Fig. 1a-b). The CMIP5 models broadly capture these features, however, they also show significant differences in space and magnitude between the basins of the Southern Ocean (Fig. 1). With the exception of CMCC-CESM, which shows a northerly-extended CO_2 outgassing band between about 40^{0}S and 50^{0}S, CMIP5 models generally show the CO_2 outgassing zone between 50^{0}S – 70^{0}S, agreeing with observational estimates (Fig. 1).

The analyzed CMIP5 models have a larger spatial dispersion in the representation of the magnitudes of FCO_2 with respect to observations (Fig.1, Table 2). They generally overestimate the upwelling-driven CO_2 outgassing (55^{o}S -70^{o}S) in some basins of the Southern Ocean relative to observations. IPSL-CM5A, CanESM2, MPI-ESM, GFDL-ESM2M and MRI-ESM, for example, show CO_2 outgassing fluxes up to 25 g m^{-2} yr^{-1}, while observations only reach a maximum of 8 g m^{-2} yr^{-1} (Fig. 1). Between about 40^{o}S - 55^{o}S (Sub-

Biogeosciences Discuss., https://doi.org/10.5194/bg-2017-361
Manuscript under review for journal Biogeosciences
Discussion started: 26 September 2017

Antarctic zone), both observations and CMIP5 models largely agree, showing a CO_2 in-gassing feature which is mainly attributable to biological processes (McNeil et al., 2007; Takahashi et al., 2012). South of 65°S, in the MIZ, models generally show an excessive CO_2 in-gassing with respect to observations (with the exception of CanESM2, IPSL-CM5A-MR and CNRM-CM5). Note that as much as this bias might be a true divergence of CMIP5 models from the observed ocean, it may also be due to the lack of observations in this region, especially during the winter season (Bakker et al., 2014; Monteiro, 2010).

The Pattern Correlation Coefficient (PCC) and the Root Mean Square Error (RMSE) presented in Table 2 have been used to quantify the model performances. Out of the 10 models, 6 show a moderate spatial correlation with observations (PCC ~ 0.40 – 0.60), i.e. CNRM-CM5, GFDL-ESM2M, HadGEM2-ES, IPSL-CM5A-MR, CESM1-BGC, NorESM2 and CanESM2. While MPI-ESM-MR (PCC = 0.37), MRI-ESM (PCC = 0.36) and CMCC-CESM (PCC = -0.09) show a weak to null spatial correlation with observations, the latter mainly due to the overestimated outgassing region.

NorESM2 and CESM1-BGC are two of the ten models showing the best performance in both spatial (PCC > 0.50) and magnitude (RSME < 10) indicators. From Table 2, it is evident that an appropriate representation of the spatial properties of FCO_2 with respect to observations does not always correspond in respect of magnitudes. CanESM2 for example shows a good spatial comparison (PCC = 0.54), yet with a poor estimation of the magnitudes (RMSE = 19.5). This is thought to be caused by an overestimation of CO_2 uptake north of 55°S (≈ - 28 g m^{-2} yr^{-1}) and CO_2 outgassing (> 25 g m^{-2} yr^{-1}) in the Antarctic zone, resulting in a net Southern Ocean annual weak sink (-0.05 Pg C m^{-2} yr^{-1}). This outcome highlights the limitations of using annual mean indicators to evaluate model performance and highlights the need for a more process-based diagnostic approach.

3.2 Sea-Air CO_2 Flux Seasonal Cycle Variability and Biases

The seasonal cycle of FCO_2 is shown in Fig. 2. CMIP5 models are generally out of phase with observations as well as with each other (e.g. Anav et al., 2013). Based on the phase, the seasonality of FCO_2 in CMIP5 models can be a priori divided in two main groups: group A comprising of MPI-ESM, HadGEM-ES and NorESM, and group B, the remainder i.e. GFDL-ESM2M, CMCC-CESM, CNRM-CERFACS, IPSL-CM5A-MR, CESM1-BGC, NorESM2, MRI-ESM and CanESM2. A similar grouping was first identified by Kessler and Tjiputra, 2016. Fig. 3 presents the ensemble seasonal cycle of FCO_2 for these two groups compared to observations, with the corresponding decadal standard deviation for each ensemble in the various regions.

In the Sub-Antarctic zone for all three basins, observed FCO_2 show a weakening of CO_2 uptake during winter (less negative values in JJA) with values close to the zero flux at the onset of spring (September). Similarly, during the spring season, all three basins are seen to maintain a steady increase of CO_2 uptake until mid-summer (December), while they differ during autumn (MAM). The Pacific Ocean shows an increase in CO_2 uptake that is not observed in the other basins (only marginally in the Indian Ocean). In the Antarctic zone, the observed FCO_2 seasonal cycle is similar in all three basins (Fig. 3d-f), possibly resulting from the limited number of observations. In this region, all three basins show a weakening of CO_2 uptake from the onset of autumn (March) until mid-winter when it outgasses. This is followed by a strengthening of the CO_2 uptake throughout spring to summer when it reaches a CO_2 in-gassing peak.

The simulated seasonal cycles in the Sub-Antarctic zone (Fig. 3a-c) do not capture any basin-specific features, which is indicative of the zonal behavior seen in the spatial patterns (Fig. 1). Group A ensemble models are characterized by an exaggerated CO_2 uptake during spring-summer and CO_2 outgassing during winter. Group A models agree with observations in the phasing of CO_2 uptake during spring, but overestimate the magnitudes. The seasonal characteristics of group A models are more coherent with the observations in the Atlantic Ocean; showing a single CO_2 outgassing peak in winter and a CO_2 in-gassing peak in summer (Fig. 3b). The large standard deviation during the winter and spring-summer seasons in group A models shows that, though they agree in the phasing, they have some differences in magnitudes. Consequently, not all group A models outgas during winter; HadGEM-ES for example, outgasses in autumn (Fig 2a-c).

On the contrary, group B models are characterized by a CO_2 outgassing peak in mid-summer (Dec-Feb) and a CO_2 in-gassing peak at the end of autumn (March), with is out of phase with observations. These models only show the strengthened CO_2 uptake during spring in the Indian Ocean. Interestingly, the phase of group B models compares relatively well with the observed FCO_2 cycle in the Pacific Ocean, which is where group A models disagree the most with the observations (Fig. 3a-c).

In the Antarctic zone, both group A and group B models perform better than in the Sub-Antarctic zone, although the phase differences are still large (Fig. 3d-f). The values oscillate around zero with the largest disagreements occurring during summer in both groups. Group A shows an overestimation of the CO_2 uptake, while group-B shows an underestimation of CO_2 uptake with respect to observations. This disagreement is accompanied by a large standard deviation, showing some inter-model differences in magnitudes (Fig. 2d-f).

Biogeosciences Discuss., https://doi.org/10.5194/bg-2017-361
Manuscript under review for journal Biogeosciences
Discussion started: 26 September 2017

To explore individual model biases, we computed the FCO_2 seasonal amplitude biases for each model relative to observations in Fig. 4. A positive or negative bias indicates overestimation or underestimation irrespective of the sign of the flux. For each basin, the models were ranked according to their mean annual bias. Fig. 4 clearly shows that CMIP5 models have a general positive bias against observations during summer and/or autumn with the exception of group-A models in the Sub-Antarctic zone. While MRI-ESM and CMCC-CESM show a consistent positive bias for all four seasons in all three basins of the Sub-Antarctic zone, the overall model biases are not consistent with the seasons (Fig. 4a-c). This variability indicates that the disagreement with observations is not just due to a mismatch in magnitude, but may point to differences in the processes that drive the FCO_2 at a seasonal scale.

The Antarctic zone shows less difference between the groups, with a majority of small negative biases throughout the year for most models, with an exception of CanESM2 and IPSL-CM5A-MR and the MPI-ESM in autumn and winter. This harmony in the seasonal mean biases within CMIP5 and observations may be showing that CMIP5 models are relatively better at capturing the Antarctic zone FCO_2 seasonal characteristics (shows relatively smaller bias), provided that available observations are representative of the Antarctic zone FCO_2 seasonal properties.

3.3 Seasonal Scale Drivers of Sea-Air CO_2 Flux

We now examine how the two major drivers (i.e. temperature and DIC) regulate the seasonality of FCO_2 in the models following the method described in Sec. 2.3 (Mongwe et al., 2016). The monthly rates of change of SST $\left(\frac{\Delta SST}{\Delta t}\right)$ is shown in Fig. 5 and compared with observations from the World Ocean Atlas (Sec. 2.2). The timing of the switch from surface cooling $\left(\frac{\Delta SST}{\Delta t} < 0\right)$ to warming $\left(\frac{\Delta SST}{\Delta t} > 0\right)$ occurring in the transition from summer to autumn (March), and winter to spring (September) is identical in all CMIP5 models and coincides with observations in both the Sub-Antarctic and Antarctic zones (Fig. 5). However, the magnitudes of these warming and cooling rates are overestimated against the observations. These differences in the magnitude of $\frac{\Delta SST}{\Delta t}$ have important implications for the role that temperature plays as a driver of pCO_2. Given, for example, that the amplitude of $\frac{\Delta SST}{\Delta t}$ is roughly 0.5°C/month lower in the Indian Ocean compared to the other two basins, we expect a relatively weaker role of temperature in this basin. CMIP5 models may correctly simulate this relative difference between the basins, but the larger $\left|\frac{\Delta SST}{\Delta t}\right|$ magnitudes are likely to enhance the response of the pCO_2 to temperature in the Indian Ocean.

Biogeosciences Discuss., https://doi.org/10.5194/bg-2017-361
Manuscript under review for journal Biogeosciences
Discussion started: 26 September 2017

The computed $\frac{\Delta SST}{\Delta t}$ in Fig. 5 were used to estimate the equivalent rate of change of DIC driven by temperature variability using (2). The estimated $\left(\frac{\partial DIC}{\partial t}\right)_{SST}$ was then compared to the total DIC seasonal cycle $\left(\frac{\partial DIC}{\partial t}\right)$ such that when $|\left(\frac{\partial DIC}{\partial t}\right)_{SST}| > |\left(\frac{\partial DIC}{\partial t}\right)|$, the temperature dominates pCO_2 variability and conversely when $|\left(\frac{\partial DIC}{\partial t}\right)_{SST}| < |\left(\frac{\partial DIC}{\partial t}\right)|$, DIC is the dominant driver. We present this comparison for monthly means in the supplementary material S2. For this analysis we focus on the index $M_{T\text{-}DIC}$ (Sec. 2.3, eq. 3) using a seasonal time window as it simplifies the explanation (Fig. 6). A value of $M_{T\text{-}DIC} > 0$ (red) indicates periods where temperature is the dominant driver of the pCO_2 variability and when $M_{T\text{-}DIC} < 0$ (blue) DIC drives the variability of pCO_2.

The seasonal cycle of pCO_2 in the observational data is predominantly DIC-driven throughout the year in both the Sub-Antarctic and Antarctic zone (Fig. 6). Note, however, that during periods of high $|\frac{\Delta SST}{\Delta t}|$ i.e. autumn and spring, observations show moderate to weak DIC control ($M_{T\text{-}DIC}$ close to zero) in the Sub-Antarctic zone. The Antarctic is instead characterized by a stronger DIC index (mean Annual $M_{T\text{-}DIC} > 3$) except for spring Fig. 6.

The computed $M_{T\text{-}DIC}$ for CMIP5 models justifies our a priori separation between group A and group B in the Sub-Antarctic zone that was based on a visual inspection in section 3.2. It shows group A models (HadGEM-ES, NorESM2 and MPI-ESM) at the bottom of Fig. 6, indicating that these models are mainly DIC driven. All the group -B models are at the top of Fig 6, showing a stronger temperature control, particularly in the Sub-Antarctic zone (Fig. 6a-c). In the Antarctic zone $M_{T\text{-}DIC}$ magnitudes are coherent within CMIP5 models. Here CMIP5 models agree with observations showing the dominance of DIC as the main driver of pCO_2, with the exception of MRI-ESM. Note that the reduced role of temperature as a driver of pCO_2 in the Antarctic zone occurs even though $\frac{\Delta SST}{\Delta t}$ magnitudes are comparable with (sometimes greater than) the Sub-Antarctic zone (Fig. 5).

3.4 DIC Vertical Fluxes

At the onset of autumn, surface heat losses induce MLD deepening. This deepening stimulates convective mixing and thus entrainment of rich-CO_2 sub-surface DIC waters, which subsequently increases DIC concentration in the mixed layer (Metzl et al., 2006; Sallée et al., 2010).

Biogeosciences Discuss., https://doi.org/10.5194/bg-2017-361
Manuscript under review for journal Biogeosciences
Discussion started: 26 September 2017

To compute the entrainment rate as described in Sec. 2.4, we first examine the seasonal changes of MLD and its time rate of change compared with the observations (Fig. 7). Except for NorESM2 and IPSL-CM5A (in the Pacific Ocean), CMIP5 models largely agree with the observational data at the onset of MLD deepening (February in the Pacific Ocean, and March for the Atlantic and Indian Ocean) and shoaling (September) in the Sub-Antarctic zone. In the Antarctic zone CMIP5 models are largely coherent at the onset of MLD deepening (February), however significantly variable at the winter maximum depth. It worth noting that the observed MLD seasonal cycle might be biased due to limited in situ observations, more particularly during winter in the Antarctic zone (de Boyer Montégut et al., 2004).

We use the computed $\frac{\Delta MLD}{\Delta t}$ to estimate DIC entrainment fluxes (F_{DIC}) at the base of the MLD, using eq. 4. All CMIP5 models entrain subsurface DIC into the mixed layer during autumn–winter in agreement with the observational estimates (Fig. 8). The MLD rate of change is the dominant driver of F_{DIC} variability because the annual vertical profiles of DIC (S3 & S4 supplementary material) show that, in agreement with observations, the simulated DIC vertical gradients weaken below 90 m and are constant for most of the mesopelagic zone in the Sub-Antarctic zone (>100 m in the Antarctic zone). Following the smaller monthly change in MLD (~ 60 m month^{-1} vs ~ 35 m month^{-1}) (S5 Supplementary), the Antarctic zone shows comparable smaller DIC entrainment fluxes with respect to the Sub-Antarctic zone (Fig. 8). Note that while the Antarctic zone shows lower DIC entrainment fluxes compared to the Sub-Antarctic zone, it is characterized by higher DIC vertical gradients in the upper 100 m in CMIP5 models (S4 supplementary).

4. Discussion

In this study, we use a diagnostic approach from Mongwe et al., 2016 as a basis to investigate processes regulating FCO_2 at the seasonal scale in earth system models, assessing the behaviour of 10 CMIP5 ESMs against available observations in the Southern Ocean. The 10 models analyzed can be divided in two major groups (Fig. 3): Group A consisted of models that overestimate the role of the DIC as the main driver of pCO_2 (hence FCO_2), and Group B, which overestimates the role of temperature in FCO_2 seasonal variability. These two classes of CMIP5 models were first distinguished by Kessler and Tjiputra (2016). Kessler and Triputra (2016) describe how FCO_2 seasonal biases in these two groups predispose equivalent biases in the long term CO_2 projections, where, for example, models which overestimate biological CO_2 uptake result in a stronger century scale CO_2 sink. Here we investigate the drivers of FCO_2 at the seasonal scale with the aim of examining the mechanisms behind the observed biases in the Sub-Antarctic and Antarctic zones.

4.1 Sub-Antarctic zone

The diagnostics presented in Fig. 6 show that the grouping of the seasonal cycle of FCO_2 is determined by the role of temperature. Group A (bottom) and B (top) models cluster together in all the basins of the Sub-Antarctic zone with the only exception of CESM1-BGC in the Atlantic Ocean, which is closer to the Group A models. The largest values of the index of temperature dominance in Group B models are found in autumn in all basins, while the largest index of DIC-dominance is scattered between spring and autumn, depending on the basin. This indicates a major role for the transitional seasons in determining the CO_2 flux biases. CMIP5 models agree with the observed phasing of $\frac{\Delta SST}{\Delta t}$ (Fig. 5), but differences in the magnitude of these rates are particularly large for all models during periods of maximum surface warming and cooling (late summer/autumn and spring).

The diagnostics in Fig. 6 link the analyzed CO_2 outgassing feature during summer in group B models (Fig. 3a-c, Dec-Feb) to temperature as the main driver. This feature coincides with a high $\frac{\Delta SST}{\Delta t}$ (Fig 5a-c), which points to the SST driven surface CO_2 solubility as the main controlling factor for the bias. The weakening of surface CO_2 solubility as the surface ocean warms up in spring-summer turns the direction of the CO_2 flux into a source in group B models. While observations indicate that this feature may be realistic in the Pacific Ocean, it is not clearly evident in the Atlantic and Indian Oceans (Fig. 3a-c). Group A models, on the contrary, maintain a strong net CO_2 sink into summer, due to the preceding exaggerated biological uptake (DIC-driven, according to Fig. 8). With the onset of autumn, the rapid cooling of the surface ocean (Fig 5a-c) enhances the CO_2 solubility. This strengthens the CO_2 uptake and thus group B models show an overestimation of the CO_2 sink. These models are not fundamentally different from group A in terms of DIC entrainment (Fig. 8a-c), but the overwhelming temperature-driven solubility of CO_2 in the group B models (Fig. 6a-c) offsets all DIC processes, leading to the (biased) net CO_2 sink during autumn (Fig. 3a-c).

The CMIP5 models show a marked cooling (Fig. 5) and deepening of the MLD in March-June (Fig. 7) with a subsequent increase of the DIC entrainment (Fig. 8), which are all likely to be realistic processes occurring in the Southern Ocean. While surface cooling strengthens CO_2 solubility in autumn, the concurrent MLD deepening has an opposing effect (Mahadevan et al., 2011). The entrainment of rich CO_2 sub-surface waters weakens the sea-air CO_2 gradient, diminishing CO_2 ingassing and leading to outgassing in some instances (Lenton et al., 2013; Takahashi, et al 2012). However, the analyzed models are characterized by the extremes of these processes in the autumn-winter transition. Group A models show a rapid weakening of the CO_2 ingassing (summer-autumn) towards outgassing conditions in winter as a consequence of the exaggerated role of DIC entrainment in all three basins of the Sub-Antarctic zone (Fig. 3a-c). MPI-ESM, HadGEM-ES and NorESM2 have the earliest positive rate of DIC increase in late summer (Fig. 9a-c),

Biogeosciences Discuss., https://doi.org/10.5194/bg-2017-361
Manuscript under review for journal Biogeosciences
Discussion started: 26 September 2017

although this may be not totally driven by entrainment (apart from NorESM2, Fig. 8a-c). In addition to the role of mixing, we hypothesize that organic matter remineralization may contribute to the simulated increase of DIC. Given the overestimated biological production in group-A models (Fig. 9c-f), remineralization is anticipated to be high and to commence shortly after biomass reaches its maximum. This phenomenon is shown by the early (February) maximum in the surface rate of change of DIC for group A, which is contrary to the winter peak (June – July) shown by group B and observations previously linked to entrainment (e.g. Mahadevan et al., 2011; Takahashi et al., 2009) (Fig. 9d-f). Here the return of the DIC from biological activity may be rapid enough to add to the entrainment rate and completely override the temperature-driven increase of solubility. This is particularly evident in models that overestimate primary production i.e. group A models. We thus propose that the observed rapid weakening and outgassing of FCO_2 in later summer to early autumn (January – April) is most likely driven by respiration in group A models (Fig. 3)

At the onset of spring (September), the net consumption of surface CO_2 by photosynthesis enhances CO_2 uptake (Le Quéré and Saltzman, 2013). This observed CO_2 uptake is exaggerated in the group A models, but only evident in the Indian Ocean in group B models (Fig. 3a-c). Once again the model skill to display this feature is dependent on the relative strength of the rate of temperature and DIC-driven processes presented in Fig. 6a-c. Group A models are markedly driven by DIC-related processes and the partial agreement of the flux is due to the elevated (and overestimated) primary production, represented here by the seasonal cycle of chlorophyll (Fig. 9b-f). This was also suggested by Kessler and Tjiputra (2016). This overestimated primary production in group A is indicative of the high rate of change of DIC in Fig. 9 which sustains a strong DIC control $\left(\frac{\Delta DIC}{\Delta t}\right) > \left(\frac{\partial DIC}{\partial t}\right)_{SST}$. During spring, group B models show contrasting values of the index in Fig. 6a-c indicating the combined role of temperature and DIC. Models like GFDL-ESM2M and CESM1-BGC show the observed uptake flux in all three basins, while CanESM2 and CMCC-CESM display this feature only in the Indian Ocean. CMCC-CESM captures this feature in the Indian Ocean because primary production is greater in this basin (Fig. 9f), while CanESM2 does so because of the relatively lower $\frac{\Delta SST}{\Delta t}$ amplitude (Fig. 5c).

This analysis shows that while the seasonal cycle of FCO_2 in MPI-ESM, HadGEM-ES and NorESM2 is predominantly DIC-driven, CNRM-CESM and IPSL-CM5A-MR show the opposite extreme, in which temperature (solubility) completely explains the flux (Fig. 6). A balance of these two extremes is shown by CESM1-BGC (Fig. 2a-c, 5a-c), which is the model that alternates between group A and group B behaviour (Fig. 4a-c). Because the CESM1-BGC seasonal cycle of $\frac{\Delta SST}{\Delta t}$and $\frac{\Delta DIC}{\Delta t}$ are comparable to the observations in both phase and magnitude (Fig. 5 and 9), its corresponding FCO_2 seasonal variability compares better with observations in all three basins of the Sub-Antarctic zone (Fig. 2a-c). It is interesting to note that CESM1-BGC is not the model with the best annual indicators (i.e. PCC and RMSE) of performance as presented in Sec. 3.1. This is important because though annual means are useful comparison indicators, long term CO_2 changes (century scale) are based on the seasonal characteristics of the drivers of FCO_2 (Hauck and Völker, 2015; Kessler and Tjiputra, 2016). Having an observed comparable annual mean and distribution is not a guarantee of model performance: NorESM2 for example shows the highest spatial correlation (PCC = 0.60) and lowest RMSE (9.0) against observations, but lacks the proper mechanisms driving FCO_2 at the seasonal scale.

The ability of CESM1-BGC to display a relatively stronger CO_2 uptake in comparison to CMCC-CESM during spring, though CMCC-CESM exhibits a more pronounced production (high chlorophyll, Fig. 9), is noteworthy. In this case the role of temperature offsets the impact of biological CO_2 uptake. This suggests that the inability of CMIP5 models to resolve the observed FCO_2 seasonal cycle does not depend only on the limitation of the biological models (though this cannot be excluded), but rather on the sensitivity of the modeled pCO_2 to the relative seasonal contributions of the simulated FCO_2 drivers.

4.2 Antarctic zone

In the Antarctic zone, all selected CMIP5 models are in general agreement, as well as with observations on the dominant role of DIC in regulating FCO_2 seasonal cycle (Fig. 6d-f). With the exception of MRI-ESM, which shows a temperature driven FCO_2 seasonal cycle due to the exaggerated rate of temperature change in this region (Fig. 5d-f), all the other models are DIC-driven. Here both CMIP5 models and observations show little inter-basin differences in the seasonal cycle of FCO_2, suggesting that mechanisms driving FCO_2 are less localized here at the seasonal scale in comparison to the sub-Antarctic zone. While this spatial coherence in FCO_2 might be an observed feature in the Antarctic zone, we are also mindful that the emergence of basin specific spatial characteristics of FCO_2 might be inhibited by lack of observational coverage, particularly in this region (Bakker et al., 2016; Gregor et al., 2017).

The tendency of the pCO_2 to be driven by DIC instead of temperature in the Antarctic zone is a consequence of the greater amplitude of the DIC rate of change (Fig. 9d-f). GFDL-2ESM2M and CNRM-CM5, for example, show a stronger DIC index though they also exhibit more pronounced $\frac{\Delta SST}{\Delta t}$ seasonal amplitudes here relative to the Sub-Antarctic zone. These analyzed increased rates of change of DIC (relative to the Sub-Antarctic zone) are proposed to be due to surface DIC processes. As evident in Fig. 8, bottom or subsurface DIC could not be the main driver of these amplified DIC amplitudes because the

Antarctic zone shows comparable lower entrainment fluxes (Fig. 8).

As anticipated, the seasonal cycle of chlorophyll in Fig. 9 show coherence (symmetric ~ negative correlation) with the analyzed rate of change of DIC in CMIP5 models. Similarly, relatively larger $\frac{\Delta DIC}{\Delta t}$ amplitudes are depicted by group A models consistent with their concurrent chlorophyll magnitudes. This shows that chlorophyll plays a major role in the seasonal modulation of DIC and thus FCO_2 in the Antarctic zone, this is consistent with Rosso et al., 2017 findings. Note that in contrast to the Sub-Antarctic zone, the a priori model grouping applied in section 3.2 does not result in the clustering of the two model groups in Fig. 6, because almost all models are DIC driven (with the exception of MRI-ESM). However, while the seasonal cycle of FCO_2 in CMIP5 models are mostly comparable with observation during winter, group A and group B models do show some differences during summer and spring (Fig. 3), even if they are both DIC driven. This shows that while primary production is playing a major role in regulating surface DIC (and hence FCO_2), there are other processes that modulate FCO_2 at a seasonal scale. We speculate that sea-ice formation/dilution and sub-surface organic matter respiration may have an important role as suggested by Rysgaard et al., 2011 and Rosso et al 2017 and they should be investigated as part of a future study.

We have shown that the overestimation of warming and cooling rates in CMIP5 models constitute an important bias for CO_2 processes at the seasonal scale, which is a major mode of variability for CO_2 (Lenton et al., 2012). This is concerning because the seasonal characteristics of CO_2 informs long term oceanic CO_2 uptake projections in ESM (Hauck and Völker, 2015; Lenton et al., 2013). While these overestimated cooling and warming rates may cancel each other out at the seasonal scale such that the annual net heat is comparable to the observed properties, this bias is likely to affect the short term climate sensitivity in ESM. In the Antarctic zone these temperature bias is likely to influence the surface heat regulation which has a bearing on the mechanisms and properties of sea-ice (Rysgaard et al., 2011; Frölicher et al., 2015; Rosso et al 2017). Therefore these analyzed temperature bias pose an important predicament with respect to our ability to predict future earth system changes, particularly the carbon cycle. We propose this bias as an important consideration to the model developing community as it relates to future biogeochemical and CMIP ESM development.

5. Conclusions

In this analysis we used a diagnostic based on the seasonal variability of the rates of change of the drivers of CO_2 to investigate biases in the seasonal cycle of FCO_2 between 10 CMIP5 models and observations in the Southern Ocean. By examining the relative rates of change of the drivers of CO_2 at the seasonal scale

Biogeosciences Discuss., https://doi.org/10.5194/bg-2017-361
Manuscript under review for journal Biogeosciences
Discussion started: 26 September 2017

we show that the biases FCO_2 in CMIP5 models cluster into two main groups. Group A are characterized by exaggerated primary production, such that biologically driven DIC changes mainly regulate the seasonal cycle of FCO_2. Group B on the other hand overestimates the role of solubility and thus variability in temperature dominantly regulates FCO_2 changes. While CMIP5 models mostly show a dominant influence of one of these two extremes i.e. temperature and biological driven DIC changes, observations show a modest influence on both these drivers, but mostly regulated by DIC.

Compared to available observations, we find that CMIP5 models mostly overestimate the rate of surface warming at the onset of spring (OND) and the rate of cooling in autumn (MAM), Fig.5. Because of this, the influence of temperature (through CO_2 solubility) on pCO_2 is overestimated in most CMIP5 models (group B models i.e. 7 of 10). This exaggeration of solubility in the pCO_2 results in a CO_2 ingassing and outgassing bias during autumn and spring respectively in CMIP5 models. Consequently the FCO_2 seasonal cycle distortion caused by these biases is mainly responsible for the departure of group B models from observed FCO_2 constraints. Though group A models do not show these solubility driven biases (because all CMIP5 models do show overestimated $|\frac{\Delta SST}{\Delta t}|$ magnitudes against observations), we hypothesize that if the overestimated primary production could be corrected, group A models would exhibit this characteristic.

We find that though some models exhibit comparable chlorophyll magnitudes with observations during spring, the concurrent increase of CO_2 uptake (Biological CO_2 uptake) is not always observed in CMIP5 models e.g. CMCC-CESM and CESM1-BGC. Because surface warming coincides with primary production during spring, the anticipated CO_2 uptake is dependent on the extent/strength of the surface CO_2 solubility with respect to biologically driven changes in DIC. Our analysis shows that though some group B models (e.g. CMCC-CESM) have comparable chlorophyll magnitudes with group A and observations, the expected biological CO_2 uptake is diminished by solubility, given the temperature control. Decreased surface solubility weakens CO_2 uptake such that the net flux is a weak CO_2 sink. Because of this phenomenon, some models, with lower chlorophyll magnitudes, show a significant net CO_2 sink during spring when compared with observations, provided concurrent warming rates are modest (comparable to observations or lower, e.g. CESM1-BGC). This finding proposes that the inability of the CMIP5 ESMs to resolve CO_2 biological uptake during spring might be crucially related to the sensitivity of the pCO2 to temperature in addition to underestimated biological CO_2 uptake. This analysis shows that while CMIP5 models show differences in the presentation of the seasonal cycle of chlorophyll, all models show biases in rate of change of temperature which present the first order problem to solving the seasonal variability of pCO_2 and FCO_2.

Biogeosciences Discuss., https://doi.org/10.5194/bg-2017-361
Manuscript under review for journal Biogeosciences
Discussion started: 26 September 2017

References

Adachi, Y., Yukimoto, S., Deushi, M., Obata, A., Nakano, H., Tanaka, T. Y., Hosaka, M., Sakami, T., Yoshimura, H., Hirabara, M., Shindo, E., Tsujino, H., Mizuta, R., Yabu, S., Koshiro, T., Ose, T. and Kitoh, A.: Basic performance of a new earth system model of the Meteorological Research Institute, Pap. Meteorol. Geophys., 64, 1–19, doi:10.2467/mripapers.64.1, 2013.

Bakker, D. C. E., Pfeil, B., Smith, K., Hankin, S., Olsen, a., Alin, S. R., Cosca, C., Harasawa, S., Kozyr, a., Nojiri, Y., O'Brien, K. M., Schuster, U., Telszewski, M., Tilbrook, B., Wada, C., Akl, J., Barbero, L., Bates, N. R., Boutin, J., Bozec, Y., Cai, W. J., Castle, R. D., Chavez, F. P., Chen, L., Chierici, M., Currie, K., De Baar, H. J. W., Evans, W., Feely, R. a., Fransson, a., Gao, Z., Hales, B., Hardman-Mountford, N. J., Hoppema, M., Huang, W. J., Hunt, C. W., Huss, B., Ichikawa, T., Johannessen, T., Jones, E. M., Jones, S. D., Jutterström, S., Kitidis, V., Körtzinger, a., Landschützer, P., Lauvset, S. K., Lefèvre, N., Manke, a. B., Mathis, J. T., Merlivat, L., Metzl, N., Murata, a., Newberger, T., Omar, a. M., Ono, T., Park, G. H., Paterson, K., Pierrot, D., Ríos, a. F., Sabine, C. L., Saito, S., Salisbury, J., S. Sarma, V. V. S., Schlitzer, R., Sieger, R., Skjelvan, I., Steinhoff, T., Sullivan, K. F., Sun, H., Sutton, a. J., Suzuki, T., Sweeney, C., Takahashi, T., Tjiputra, J., Tsurushima, N., C. Van Heuven, S. M. a, Vandemark, D., Vlahos, P., Wallace, D. W. R., Wanninkhof, R. and Watson, a. J.: An update to the surface ocean CO_2 atlas (SOCAT version 2), Earth Syst. Sci. Data, 6(1), 69–90, doi:10.5194/essd-6-69-2014, 2014.

Bakker, D. C. E., Pfeil, B., Landa, C. S., Metzl, N., O'Brien, K. M., Olsen, A., Smith, K., Cosca, C., Harasawa, S., Jones, S. D., Nakaoka, S. I., Nojiri, Y., Schuster, U., Steinhoff, T., Sweeney, C., Takahashi, T., Tilbrook, B., Wada, C., Wanninkhof, R., Alin, S. R., Balestrini, C. F., Barbero, L., Bates, N. R., Bianchi, A. A., Bonou, F., Boutin, J., Bozec, Y., Burger, E. F., Cai, W. J., Castle, R. D., Chen, L., Chierici, M., Currie, K., Evans, W., Featherstone, C., Feely, R. A., Fransson, A., Goyet, C., Greenwood, N., Gregor, L., Hankin, S., Hardman-Mountford, N. J., Harlay, J., Hauck, J., Hoppema, M., Humphreys, M. P., Hunt, C. W., Huss, B., Ibánhez, J. S. P., Johannessen, T., Keeling, R., Kitidis, V., Körtzinger, A., Kozyr, A., Krasakopoulou, E., Kuwata, A., Landschützer, P., Lauvset, S. K., Lefèvre, N., Lo Monaco, C., Manke, A., Mathis, J. T., Merlivat, L., Millero, F. J., Monteiro, P. M. S., Munro, D. R., Murata, A., Newberger, T., Omar, A. M., Ono, T., Paterson, K., Pearce, D., Pierrot, D., Robbins, L. L., Saito, S., Salisbury, J., Schlitzer, R., Schneider, B., Schweitzer, R., Sieger, R., Skjelvan, I., Sullivan, K. F., Sutherland, S. C., Sutton, A. J., Tadokoro, K., Telszewski, M., Tuma, M., Van Heuven, S. M. A. C., Vandemark, D., Ward, B., Watson, A. J. and Xu, S.: A multi-decade record of high-quality fCO_2 data in version 3 of the Surface Ocean CO_2 Atlas (SOCAT), Earth Syst. Sci. Data, 8(2), 383–413, doi:10.5194/essd-8-383-2016, 2016.

Barbero, L., Boutin, J., Merlivat, L., Martin, N., Takahashi, T., Sutherland, S. C. and Wanninkhof, R.: Importance of water mass formation regions for the air-sea CO2 flux estimate in the southern ocean, Global Biogeochem. Cycles, 25(1), 1–16, doi:10.1029/2010GB003818, 2011.

de Boyer Montégut, C., Madec, G., Fischer, A. S., Lazar, A. and Iudicone, D.: Mixed layer depth over the global ocean: An examination of profile data and a profile-based climatology, J. Geophys. Res. C Ocean., 109(12), 1–20, doi:10.1029/2004JC002378, 2004.

Dufour, C. O., Sommer, J. Le, Gehlen, M., Orr, J. C., Molines, J. M., Simeon, J. and Barnier, B.: Eddy compensation and controls of the enhanced sea-to-air CO2 flux during positive phases of the Southern Annular Mode, Global Biogeochem. Cycles, 27(3), 950–961, doi:10.1002/gbc.20090, 2013.

Dunne, J. P., John, J. G., Shevliakova, S., Stouffer, R. J., Krasting, J. P., Malyshev, S. L., Milly, P. C. D., Sentman, L. T., Adcroft, A. J., Cooke, W., Dunne, K. A., Griffies, S. M., Hallberg, R. W., Harrison, M. J., Levy, H., Wittenberg, A. T., Phillips, P. J. and Zadeh, N.: GFDL's ESM2 global coupled climate-carbon earth system models. Part II: Carbon system formulation and baseline simulation characteristics, J. Clim., 26(7), 2247–2267, doi:10.1175/JCLI-D-12-00150.1, 2013.

Frölicher, T. L., Sarmiento, J. L., Paynter, D. J., Dunne, J. P., Krasting, J. P. and Winton, M.: Dominance of the Southern Ocean in Anthropogenic Carbon and Heat Uptake in CMIP5 Models, J. Clim., 28(2), 862–886, doi:10.1175/JCLI-D-14-00117.1, 2015.

Fujita, D., Ishizawa, M., Maksyutov, S., Thornton, P. E., Saeki, T. and Nakazzawa, T.: Inter-annual variability of the atmospheric carbon dioxide concentrations as simulated with global terrestrial biosphere models and an atmospheric transport model, Tellus, 55B, 530–546, 2003.

Fung, I. Y., Doney, S. C., Lindsay, K. and John, J.: Evolution of carbon sinks in a changing climate., Proc. Natl. Acad. Sci. U. S. A., 102(32), 11201–11206, doi:10.1073/pnas.0504949102, 2005.

Gregor, L., Kok, S. and Monteiro, P. M. S.: Empirical methods for the estimation of Southern Ocean CO 2 : Support Vector and Random Forest Regression, , (June), 1–18, 2017.

Gruber, N., Gloor, M., Mikaloff Fletcher, S. E., Doney, S. C., Dutkiewicz, S., Follows, M. J., Gerber, M., Jacobson, A. R., Joos, F., Lindsay, K., Menemenlis, D., Mouchet, A., Müller, S. a., Sarmiento, J. L. and

Takahashi, T.: Oceanic sources, sinks, and transport of atmospheric CO2, Global Biogeochem. Cycles, 23(1), 1–21, doi:10.1029/2008GB003349, 2009.

Hauck, J. and Völker, C.: Rising atmospheric CO2 leads to large impact of biology on Southern Ocean CO2 uptake via changes of the Revelle factor, Geophys. Res. Lett., 42(5), 1459–1464, doi:10.1002/2015GL063070, 2015.

Hauck, J., Völker, C., Wolf-Gladrow, D. a., Laufkötter, C., Vogt, M., Aumont, O., Bopp, L., Buitenhuis, E. T., Doney, S. C., Dunne, J., Gruber, N., John, J., Le Quéré, C., Lima, I. D., Nakano, H. and Totterdell, I.: On the Southern Ocean CO2 uptake and the role of the biological carbon pump in the 21st century, Global Biogeochem. Cycles, 29, 1451–1470, doi:doi:10.1002/2015GB005140, 2015.

Ilyina, T., Six, K. D., Segschneider, J., Maier-Reimer, E., Li, H. and Núñez-Riboni, I.: Global ocean biogeochemistry model HAMOCC: Model architecture and performance as component of the MPI-Earth system model in different CMIP5 experimental realizations, J. Adv. Model. Earth Syst., 5(2), 287–315, doi:10.1029/2012MS000178, 2013.

Kessler, A. and Tjiputra, J.: The Southern Ocean as a constraint to reduce uncertainty in future ocean carbon sinks, Earth Syst. Dyn., 7(2), 295–312, doi:10.5194/esd-7-295-2016, 2016.

Key, R. M., Kozyr, A., Sabine, C. L., Lee, K., Wanninkhof, R., Bullister, J. L., Feely, R. A., Millero, F. J., Mordy, C. and Peng, T. H.: A global ocean carbon climatology: Results from Global Data Analysis Project (GLODAP), Global Biogeochem. Cycles, 18(4), 1–23, doi:10.1029/2004GB002247, 2004.

Landschützer, P., Gruber, N., Bakker, D. C. E., Schuster, U., Nakaoka, S., Payne, M. R., Sasse, T. P. and Zeng, J.: A neural network-based estimate of the seasonal to inter-annual variability of the Atlantic Ocean carbon sink, Biogeosciences, 10(11), 7793–7815, doi:10.5194/bg-10-7793-2013, 2013.

Lee, K., Tong, L. T., Millero, F. J., Sabine, C. L., Dickson, A. G., Goyet, C., Park, G. H., Wanninkhof, R., Feely, R. a. and Key, R. M.: Global relationships of total alkalinity with salinity and temperature in surface waters of the world's oceans, Geophys. Res. Lett., 33(19), 1–5, doi:10.1029/2006GL027207, 2006.

Lenton, a., Tilbrook, B., Law, R. M., Bakker, D., Doney, S. C., Gruber, N., Ishii, M., Hoppema, M., Lovenduski, N. S., Matear, R. J., McNeil, B. I., Metzl, N., Fletcher, S. E. M., Monteiro, P. M. S., Rödenbeck, C., Sweeney, C. and Takahashi, T.: Sea-air CO2 fluxes in the Southern Ocean for the period 1990-2009, Biogeosciences, 10(6), 4037–4054, doi:10.5194/bg-10-4037-2013, 2013.

Locarnini, R. A., Mishonov, A. V, Antonov, J. I., Boyer, T. P., Garcia, H. E., Baranova, M. M., Zweng, M. M., Paver, C. R., Reagan, J. R., Johnson, D. R., Hamilton, M. and Seidov, D.: World Ocean Atlas 2013, NOAA Atlas, 1, 1–40, doi:10.1182/blood-2011-06-357442, 2013.

Mahadevan, A., Tagliabue, A., Bopp, L., Lenton, A., Mémery, L. and Lévy, M.: Impact of episodic vertical fluxes on sea surface pCO2, Philos. Trans. R. Soc. London A Math. Phys. Eng. Sci., 369(1943), 2009–2025, doi:10.1098/rsta.2010.0340, 2011.

McNeil, B. I., Metzl, N., Key, R. M., Matear, R. J. and Corbiere, A.: An empirical estimate of the Southern Ocean air-sea CO2 flux, Global Biogeochem. Cycles, 21(3), 1–16, doi:10.1029/2007GB002991, 2007.

Metzl, N.: Decadal increase of oceanic carbon dioxide in Southern Indian Ocean surface waters (1991-2007), Deep. Res. Part II Top. Stud. Oceanogr., 56(8–10), 607–619, doi:10.1016/j.dsr2.2008.12.007, 2009.

Metzl, N., Brunet, C., Jabaud-Jan, A., Poisson, A. and Schauer, B.: Summer and winter air-sea CO2 fluxes in the Southern Ocean, Deep. Res. Part I Oceanogr. Res. Pap., 53(9), 1548–1563, doi:10.1016/j.dsr.2006.07.006, 2006.

Monteiro, P. M. S.: A Global Sea Surface Carbon Observing System: Assessment of Changing Sea Surface CO2 and Air-Sea CO2 Fluxes, Proc. Ocean. Sustain. Ocean Obs. Inf. Soc., (1), 702–714, doi:10.5270/OceanObs09.cwp.64, 2010.

Moore, J. K., Doney, S. C. and Lindsay, K.: Upper ocean ecosystem dynamics and iron cycling in a global three-dimensional model, Global Biogeochem. Cycles, 18(4), 1–21, doi:10.1029/2004GB002220, 2004.

Orsi, A. H., Whitworth, T. and Nowlin, W. D.: On the meridional extent and fronts of the Antarctic Circumpolar Current, Deep. Res. Part I, 42(5), 641–673, doi:10.1016/0967-0637(95)00021-W, 1995.

Palmer, J. R. and Totterdell, I. J.: Production and export in a global ocean ecosystem model, Deep. Res. Part I Oceanogr. Res. Pap., 48(5), 1169–1198, doi:10.1016/S0967-0637(00)00080-7, 2001.

Pasquer, B., Metzl, N., Goosse, H. and Lancelot, C.: What drives the seasonality of air–sea CO2 fluxes in the ice-free zone of the Southern Ocean: A 1D coupled physical–biogeochemical model approach, Mar. Chem., 177, 554–565, doi:10.1016/j.marchem.2015.08.008, 2015.

Le Quere, C., Andrew, R. M., Canadell, J. G., Sitch, S., Ivar Korsbakken, J., Peters, G. P., Manning, A. C., Boden, T. A., Tans, P. P., Houghton, R. A., Keeling, R. F., Alin, S., Andrews, O. D., Anthoni, P., Barbero, L., Bopp, L., Chevallier, F., Chini, L. P., Ciais, P., Currie, K., Delire, C., Doney, S. C., Friedlingstein, P., Gkritzalis, T., Harris, I., Hauck, J., Haverd, V., Hoppema, M., Klein Goldewijk, K., Jain, A. K., Kato, E., Kortzinger, A., Landschutzer, P., Lefevre, N., Lenton, A., Lienert, S., Lombardozzi, D., Melton, J. R., Metzl, N., Millero, F., Monteiro, P. M. S., Munro, D. R., Nabel, J. E. M. S., Nakaoka, S. I., O'Brien, K., Olsen, A., Omar, A. M., Ono, T., Pierrot, D., Poulter, B., Rodenbeck, C., Salisbury, J., Schuster, U., Schwinger, J., Seferian, R., Skjelvan, I., Stocker, B. D., Sutton, A. J., Takahashi, T., Tian, H., Tilbrook, B., Van Der Laan-Luijkx, I. T., Van Der Werf, G. R., Viovy, N., Walker, A. P., Wiltshire, A. J. and Zaehle, S.: Global Carbon Budget 2016, Earth Syst. Sci. Data, 8(2), 605–649, doi:10.5194/essd-8-605-2016, 2016.

Le Quéré, C. and Saltzman, E. S.: Surface Ocean-Lower Atmosphere Processes., 2013.

Rosso, I., Mazloff, M. R., Verdy, A. and Talley, L. D.: Space and time variability of the Southern Ocean carbon budget, J. Geophys. Res. Ocean., TBD(TBD), TBD, doi:10.1002/2016JC012646, 2017.

Rysgaard, S., Bendtsen, J., Delille, B., Dieckmann, G. S., Glud, R. N., Kennedy, H., Mortensen, J., Papadimitriou, S., Thomas, D. N. and Tison, J. L.: Sea ice contribution to the air-sea CO2 exchange in the Arctic and Southern Oceans, Tellus, Ser. B Chem. Phys. Meteorol., 63(5), 823–830, doi:10.1111/j.1600-0889.2011.00571.x, 2011.

Sallée, J.-B., Speer, K., Rintoul, S. and Wijffels, S.: Southern Ocean Thermocline Ventilation, J. Phys. Oceanogr., 40(3), 509–529, doi:10.1175/2009JPO4291.1, 2010.

Sallée, J. B., Wienders, N., Speer, K. and Morrow, R.: Formation of subantarctic mode water in the southeastern Indian Ocean, Ocean Dyn., 56(5–6), 525–542, doi:10.1007/s10236-005-0054-x, 2006.

Sallée, J. B., Shuckburgh, E., Bruneau, N., Meijers, a. J. S., Bracegirdle, T. J. and Wang, Z.: Assessment of Southern Ocean mixed-layer depths in CMIP5 models: Historical bias and forcing response, J. Geophys. Res. Ocean., 118(4), 1845–1862, doi:10.1002/jgrc.20157, 2013.

Sarmiento, J. L. and Gruber, N.: Ocean Biogeochemical Dynamics, Carbon N. Y., 67, doi:10.1063/1.2754608, 2006.

Séférian, R., Bopp, L., Gehlen, M., Orr, J. C., Ethé, C., Cadule, P., Aumont, O., Salas y Mélia, D., Voldoire, A. and Madec, G.: Skill assessment of three earth system models with common marine biogeochemistry, Clim. Dyn., 40(9–10), 2549–2573, doi:10.1007/s00382-012-1362-8, 2013.

Takahashi, T., Sutherland, S. C., Wanninkhof, R., Sweeney, C., Feely, R. a., Chipman, D. W., Hales, B., Friederich, G., Chavez, F., Sabine, C., Watson, A., Bakker, D. C. E., Schuster, U., Metzl, N., Yoshikawa-Inoue, H., Ishii, M., Midorikawa, T., Nojiri, Y., Körtzinger, A., Steinhoff, T., Hoppema, M., Olafsson, J., Arnarson, T. S., Tilbrook, B., Johannessen, T., Olsen, A., Bellerby, R., Wong, C. S., Delille, B., Bates, N. R. and de Baar, H. J. W.: Climatological mean and decadal change in surface ocean pCO2, and net sea-air CO2 flux over the global oceans, Deep. Res. Part II Top. Stud. Oceanogr., 56(8–10), 554–577, doi:10.1016/j.dsr2.2008.12.009, 2009.

Takahashi, T., Sweeney, C., Hales, B., Chipman, D., Newberger, T., Goddard, J., Iannuzzi, R. and Sutherland, S.: The Changing Carbon Cycle in the Southern Ocean, Oceanography, 25(3), 26–37, doi:10.5670/oceanog.2012.71, 2012.

Tjiputra, J. F., Roelandt, C., Bentsen, M., Lawrence, D. M., Lorentzen, T., Schwinger, J., Seland, Ø. and Heinze, C.: Evaluation of the carbon cycle components in the Norwegian Earth System Model (NorESM), Geosci. Model Dev. Discuss., 6(2), 301–325, doi:10.5194/gmd-6-301-2013, 2013.

Vichi, M., Pinardi, N. and Masina, S.: A generalized model of pelagic biogeochemistry.for the global ocean ecosystem. Part I: Theory, J. Mar. Syst., 64(1–4), 89–109, doi:DOI 10.1016/j.jmarsys.2006.03.006, 2007.

Wanninkhof, R., Asher, W. E., Ho, D. T., Sweeney, C. and McGillis, W. R.: Advances in quantifying air-sea gas exchange and environmental forcing., Ann. Rev. Mar. Sci., 1, 213–244, doi:10.1146/annurev.marine.010908.163742, 2009.

Zahariev, K., Christian, J. R. and Denman, K. L.: Preindustrial, historical, and fertilization simulations using a global ocean carbon model with new parameterizations of iron limitation, calcification, and N2 fixation, Prog. Oceanogr., 77(1), 56–82, doi:10.1016/j.pocean.2008.01.007, 2008.

Biogeosciences Discuss., https://doi.org/10.5194/bg-2017-361
Manuscript under review for journal Biogeosciences
Discussion started: 26 September 2017

Biogeosciences
Discussions
Open Access

Figures

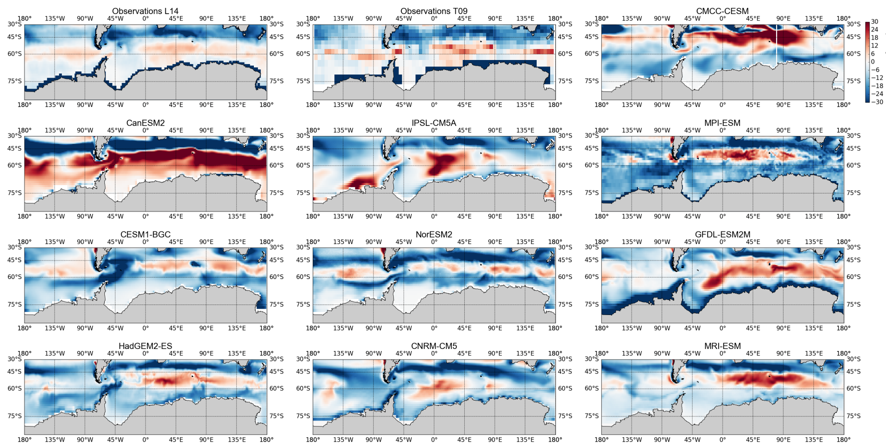

Fig. 1: Annual climatological Sea-Air CO_2 Flux (FCO_2, in gC m^{-2} yr^{-1}) for observations (L14:Landschützer et al., 2014 and T09: Takahashi et al., 2009) and 10 CMIP5 models over 1995 – 2005.

Biogeosciences Discuss., https://doi.org/10.5194/bg-2017-361
Manuscript under review for journal Biogeosciences
Discussion started: 26 September 2017

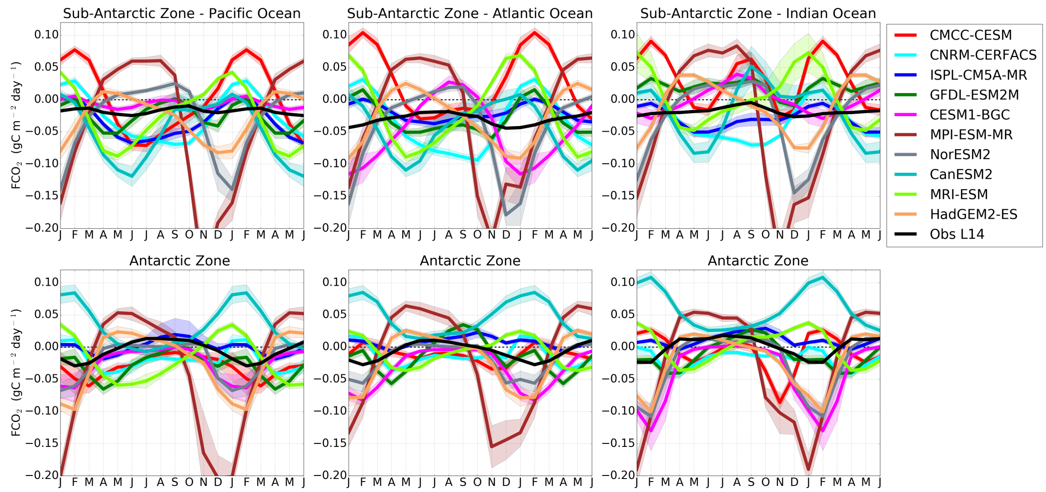

Fig. 2: Seasonal cycle of Sea-Air CO_2 Flux (FCO_2, in gC m^{-2} yr^{-1}) in observations and 10 CMIP5 models in the Sub-Antarctic and Antarctic zones of the Pacific Ocean (first column), Atlantic Ocean (second column) and Indian Ocean (third column). The shaded area shows the temporal standard deviation over the considered period (1995 – 2005).

Biogeosciences Discuss., https://doi.org/10.5194/bg-2017-361
Manuscript under review for journal Biogeosciences
Discussion started: 26 September 2017

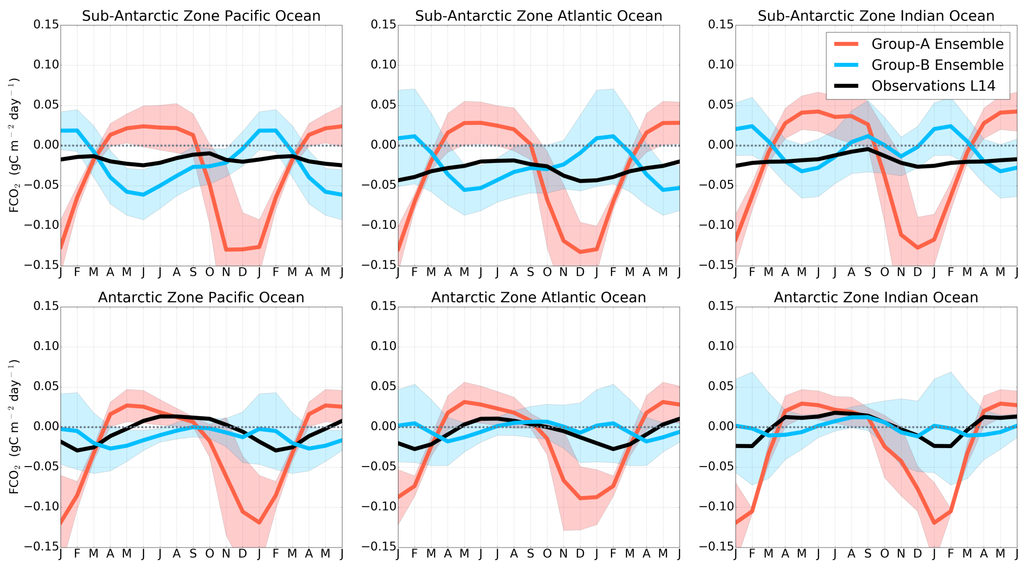

Fig. 3. Seasonal cycle of the equally weighted ensemble means of FCO_2 (gC m^{-2} yr^{-1}) from Fig. 2 for group-A models (MPI-ESM, HadGEM-ES and NorESM), and group-B models (GFDL-ESM2M, CMCC-CESM, CNRM-CERFACS, IPSL-CM5A-MR, CESM1-BGC, NorESM2, MRI-ESM and CanESM2). The shaded areas show the ensemble standard deviation. The black line is the Landschützer et al., (2014) observations.

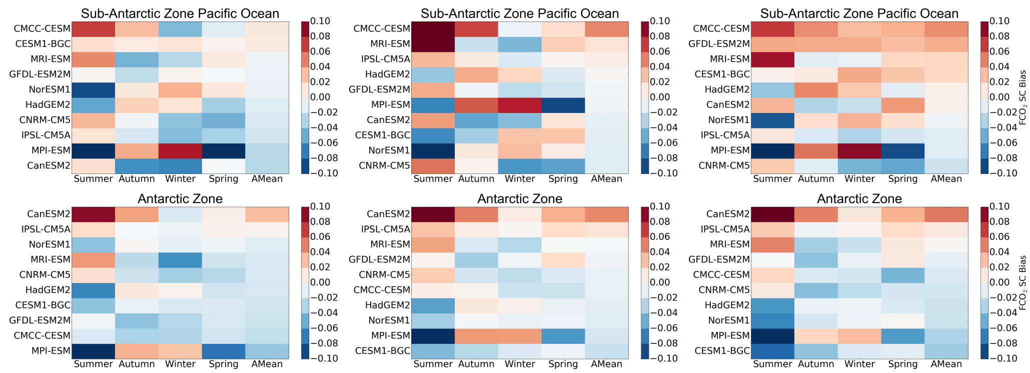

Fig. 4: Sea-Air CO_2 Flux mean seasonal and annual biases with respect to observations (gC m^{-2} yr^{-1}) for the Sub-Antarctic and Antarctic zones in the Pacific Ocean (first column, a and d), Atlantic Ocean (second column, b and e) and Indian Ocean (third column, c and f). CO_2 out-gassing biases are in red, while blue color intensity shows in-gassing biases. The models are sorted according to the annual mean bias presented in the last column (Amean).

Biogeosciences Discuss., https://doi.org/10.5194/bg-2017-361
Manuscript under review for journal Biogeosciences
Discussion started: 26 September 2017

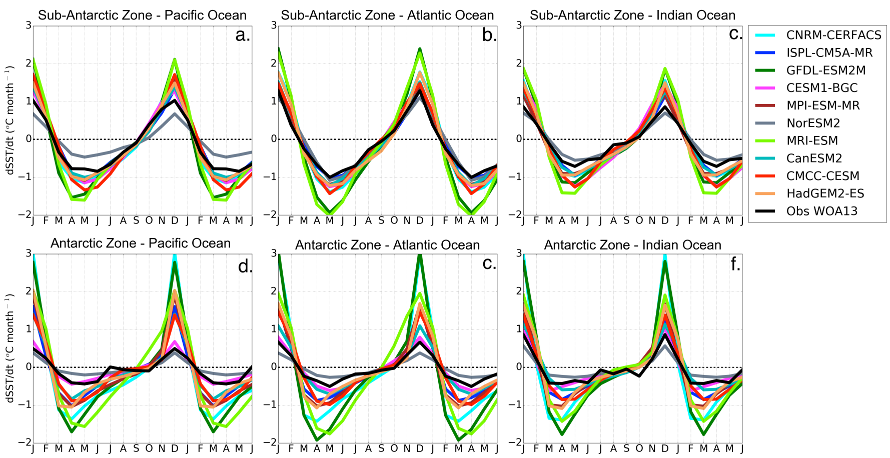

Fig. 5: Mean seasonal cycle of the estimated rate of change of sea surface temperature (ΔSST/Δt, °C month^{-1}) for the Sub-Antarctic and Antarctic zones of the Pacific Ocean (first column), Atlantic Ocean (second column) and Indian Ocean (third column).

Biogeosciences Discuss., https://doi.org/10.5194/bg-2017-361
Manuscript under review for journal Biogeosciences
Discussion started: 26 September 2017

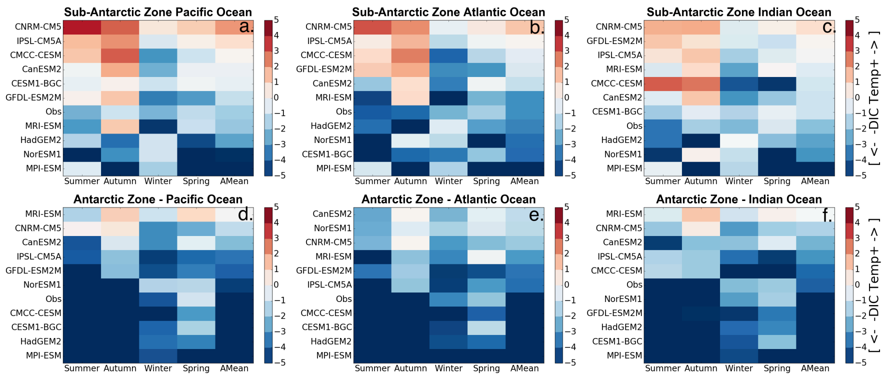

Fig. 6: Mean seasonal and annual values of the DIC–temperature control index ($M_{T\text{-}DIC}$). The increase in the red color intensity indicates increase in the strength of the temperature driver and the blue intensity shows the strength of the DIC driver. The models are sorted according to the annual mean value of the indicator presented in the last column (Amean)

Biogeosciences Discuss., https://doi.org/10.5194/bg-2017-361
Manuscript under review for journal Biogeosciences
Discussion started: 26 September 2017

Biogeosciences
Discussions
Open Access

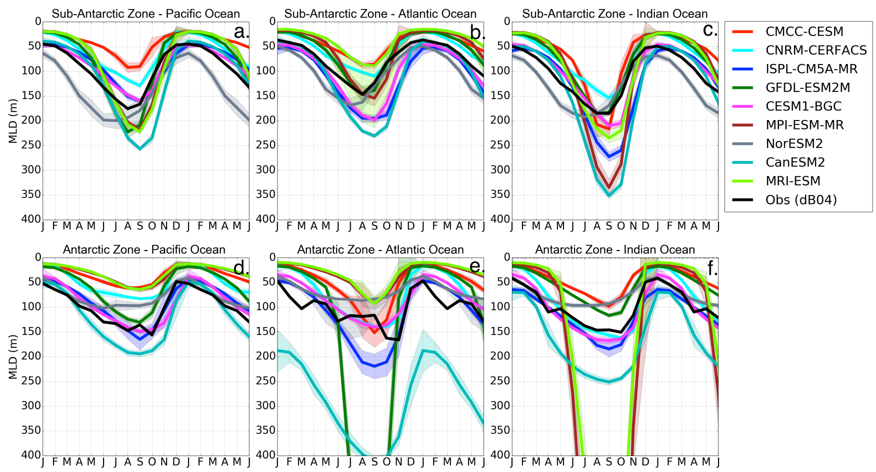

Fig. 7: Seasonal cycle of the Mixed Layer Depth (MLD) in the Sub-Antarctic and Antarctic zones of the Pacific Ocean (first column), Atlantic Ocean (second column) and Indian Ocean (third column).

Biogeosciences Discuss., https://doi.org/10.5194/bg-2017-361
Manuscript under review for journal Biogeosciences
Discussion started: 26 September 2017

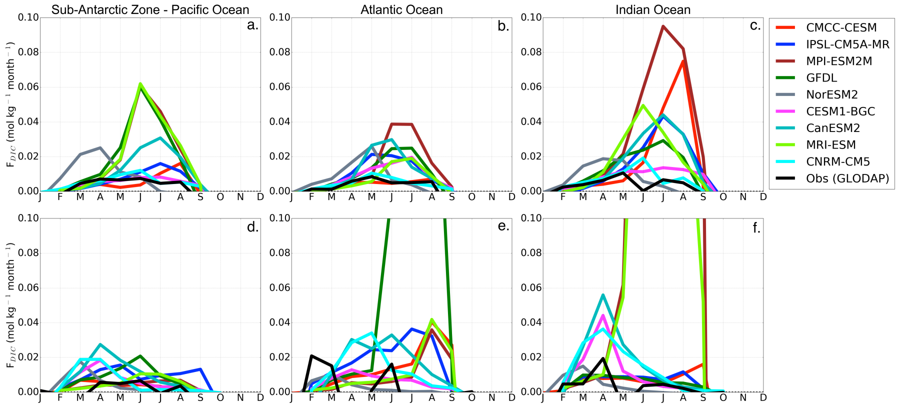

Fig. 8: Estimated DIC entrainment fluxes (mol kg month^{-1}) at the base of the mixed layer in the Sub-Antarctic and Antarctic zone of the Pacific Ocean (first column), Atlantic Ocean (second column) and Indian Ocean (third column).

Biogeosciences Discuss., https://doi.org/10.5194/bg-2017-361
Manuscript under review for journal Biogeosciences
Discussion started: 26 September 2017

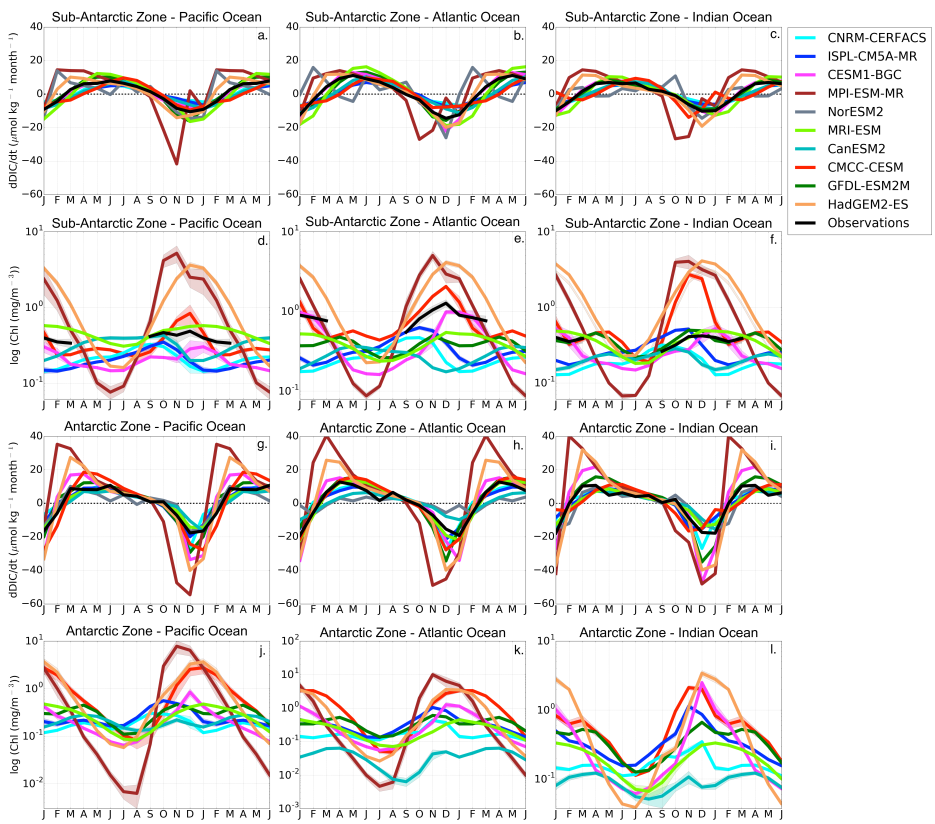

Fig. 9: Seasonal cycle of the rate of change of DIC (μmol kg month^{-1}) and chlorophyll (mg m^{-3}) at the surface ocean in the Sub-Antarctic and Antarctic zone of the Pacific Ocean (first column), Atlantic Ocean (second column) and Indian Ocean (third column).

Biogeosciences Discuss., https://doi.org/10.5194/bg-2017-361
Manuscript under review for journal Biogeosciences
Discussion started: 26 September 2017

Table 2: Sea-Air CO_2 fluxes (Pg C yr^{-1}) annual mean uptake in the Southern Ocean (first column), here defined as south of the Sub-tropical front, Sub-Antarctic zone (second column) and Antarctic zone (third column). The third and forth column shows the Pattern Correlation Coefficient (PCC) and Root Mean Square Error (RMSE) for the whole Southern Ocean for each model.

Biogeosciences Discuss., https://doi.org/10.5194/bg-2017-361
Manuscript under review for journal Biogeosciences
Discussion started: 26 September 2017

Table 2: Sea-Air CO_2 Fluxes Mean Annual Uptake, PCC and RMSE

Model	Southern Ocean	Sub-Antarctic zone	Antarctic zone	PCC	RMSE
CNRM-CM5	-0.823 ± 0.003	-0.682 ± 0.002	-0.122 ± 0.001	0.44	17.9
GFDL-ESM2M	-0.161 ± 0.005	-0.074 ± 0.004	-0.077 ± 0.002	0.43	8.47
HadGEM2-ES	-0.489 ± 0.005	-0.284 ± 0.003	-0.197 ± 0.001	0.55	10.9
IPSL-CM5A-MR	-0.496 ± 0.003	-0.582 ± 0.006	0.101 ± 0.003	0.53	10.5
MPI-ESM-MR	-0.870 ± 0.006	-0.530 ± 0.002	-0.326 ± 0.002	0.37	9.87
MRI-ESM	-0.048 ± 0.002	0.022 ± 0.003	-0.070 ± 0.001	0.36	15.6
NorESM1	-0.699 ± 0.004	-0.412 ± 0.003	-0.270 ± 0.002	0.60	8.96
CESM1-BGC	-0.532 ± 0.006	-0.132 ± 0.003	-0.385 ± 0.004	0.47	9.15
CMCC-CESM	0.121 ± 0.006	0.367 ± 0.004	-0.225 ± 0.003	-0.09	17.9
CanESM2	-0.058 ± 0.008	-0.720 ± 0.006	0.661 ± 0.004	0.54	19.5
Observations	-0.253	-0.296	0.053		